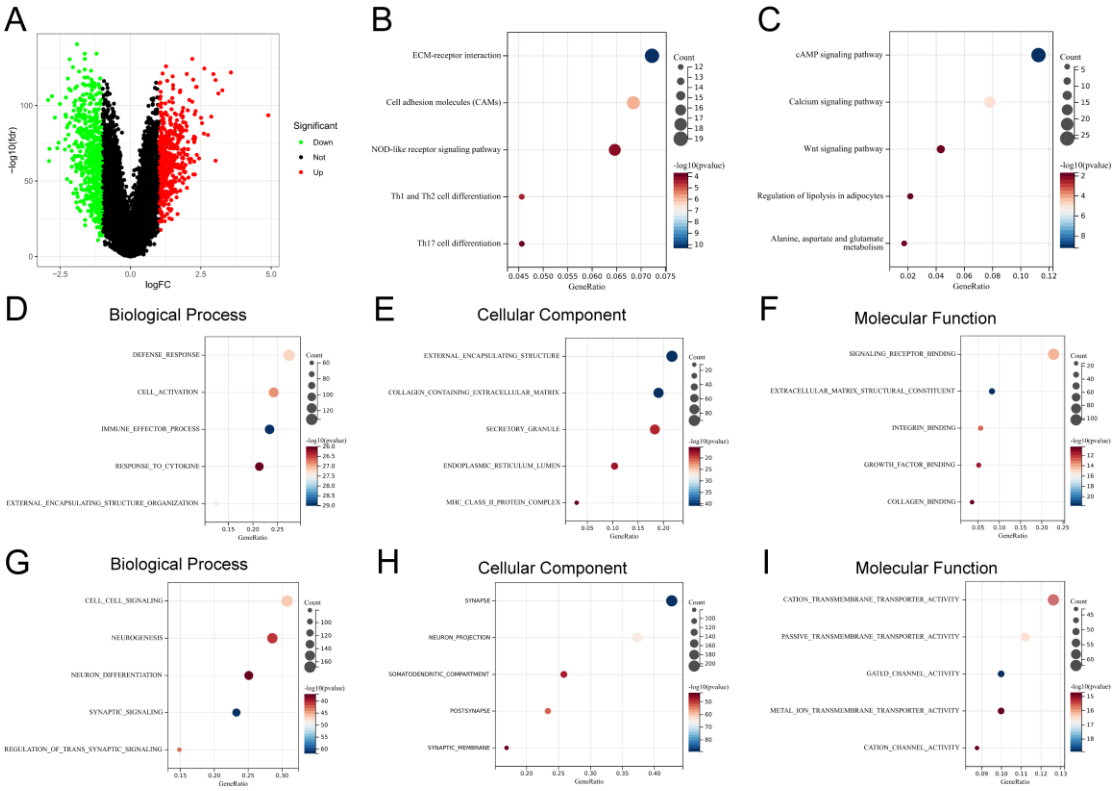

Supplementary Figure 1. Differential expression genes and functional analysis of two subgroups related to nicotinamide metabolism. (**A**) Volcano map of differentially expressed genes in two subgroups related to nicotinamide metabolism. Red and green represent differentially expressed genes up- and down-regulated by cluster1 compared to cluster2. (**B**) Bubble plots of up-regulated genes for KEGG enrichment analysis. (**C**) Bubble plots of down-regulated genes for KEGG enrichment analysis. (**D-F**) Bubble plots of up-regulated genes for GO enrichment analysis. (**G-I**) Bubble plots of down-regulated genes for GO enrichment analysis.

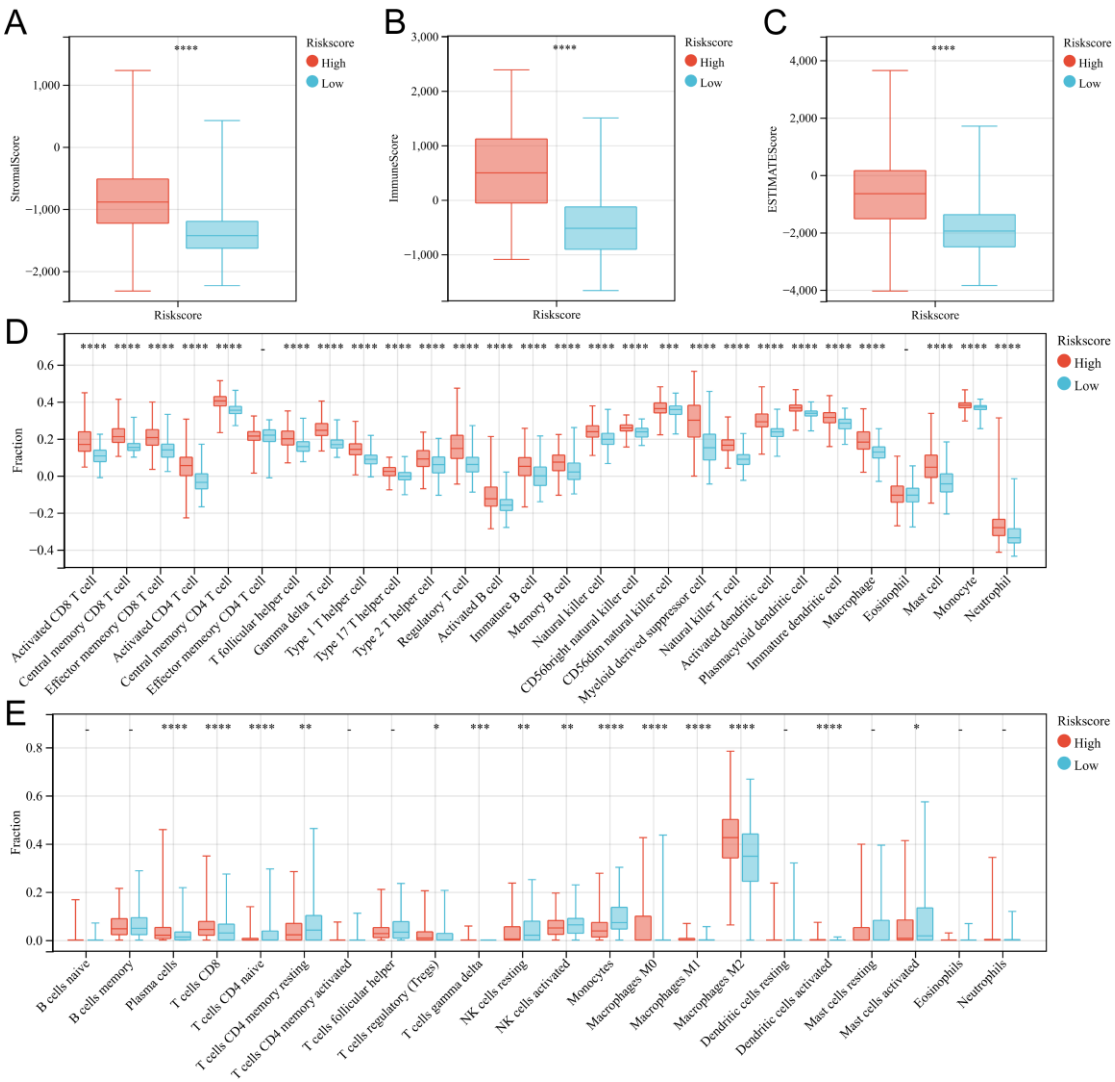

Supplementary Figure 2. Analysis of immune cell infiltration in two subgroups related to the risk score of CGGA mRNAseq693. (**A-C**) Box plot of stromal score (**A**), immune score (**B**), and ESTIMATE score (**C**) for patients in the high and low-risk score groups. (**D**)Box plot of immune cell infiltration levels high-risk score and low-risk score groups analyzed by ssGSEA. (**E**)Box plot of immune cell infiltration levels in high-risk score and low-risk score groups analyzed by CIBERSORT. *P < 0.05; **P < 0.01; ***P < 0.001, ****P < 0.0001; -, not significant.

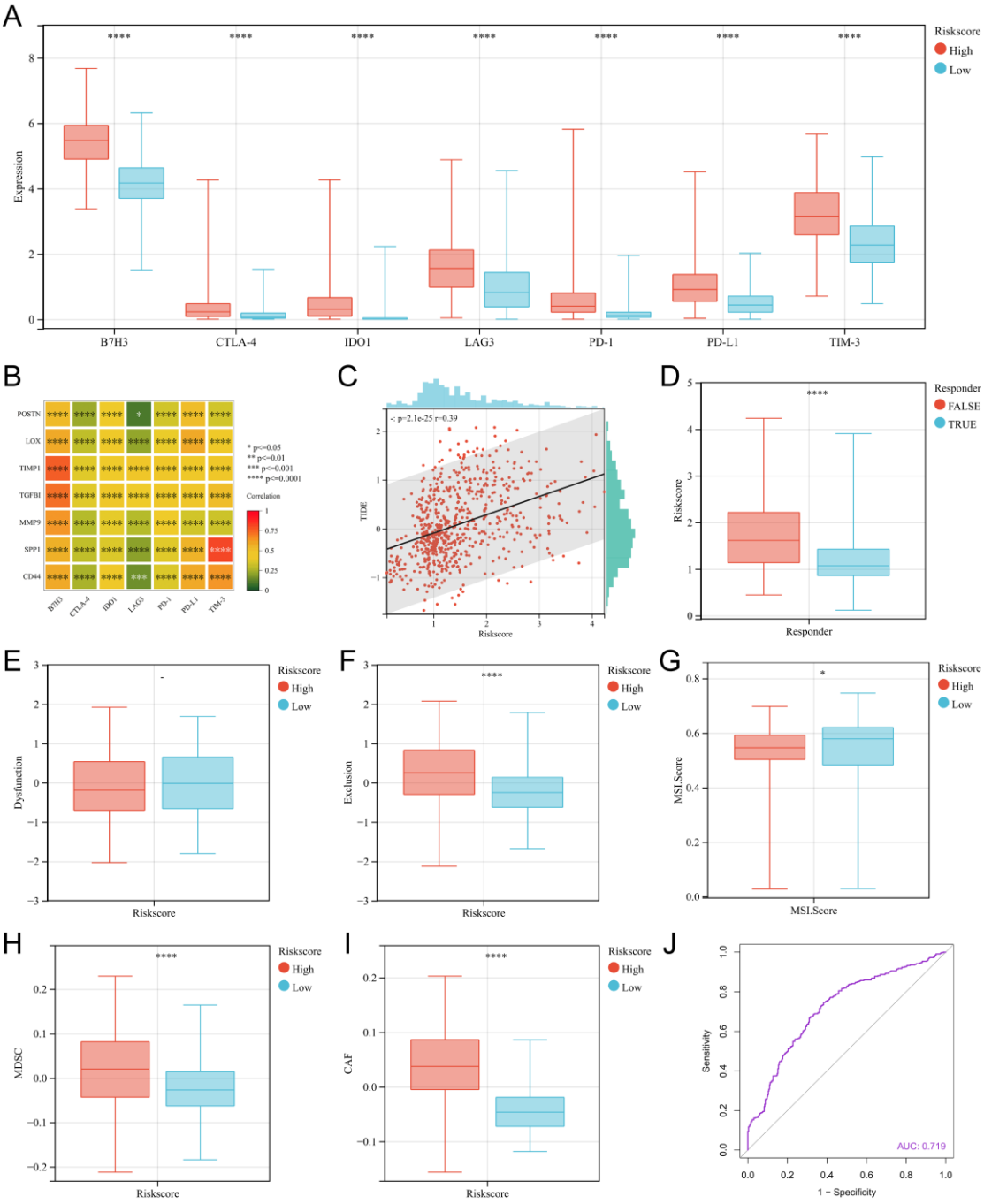

Supplementary Figure 3. The predictive role of risk model of CGGA mRNAseq693 for ICI treatment response. (**A**) Box plots of immune checkpoint expression in the high-risk score group and low-risk score group. (**B**) Correlation analysis between the expression levels of risk model-related genes and the expression levels of immune checkpoints. (**C**) Correlation analysis between the risk score and TIDE score. (**D**) Box plots of risk scores for predicting ICI treatment true responder and false responder gliomas using the TIDE algorithm. (**E**) Box plots of Dysfunction scores for high-risk score group and low-risk score group. (**F**) Box plots of Dysfunction scores for

high-risk score group and low-risk score group. (**G**) Box plot of Dysfunction scores for high-risk score group and low-risk score group. (**H**) Box plots of MDSC for high-risk score group and low-risk score group. (**I**) Box plots of CAF for high-risk score group and low-risk score group. (**J**) ROC curves of the risk score predicting response to ICI treatment.

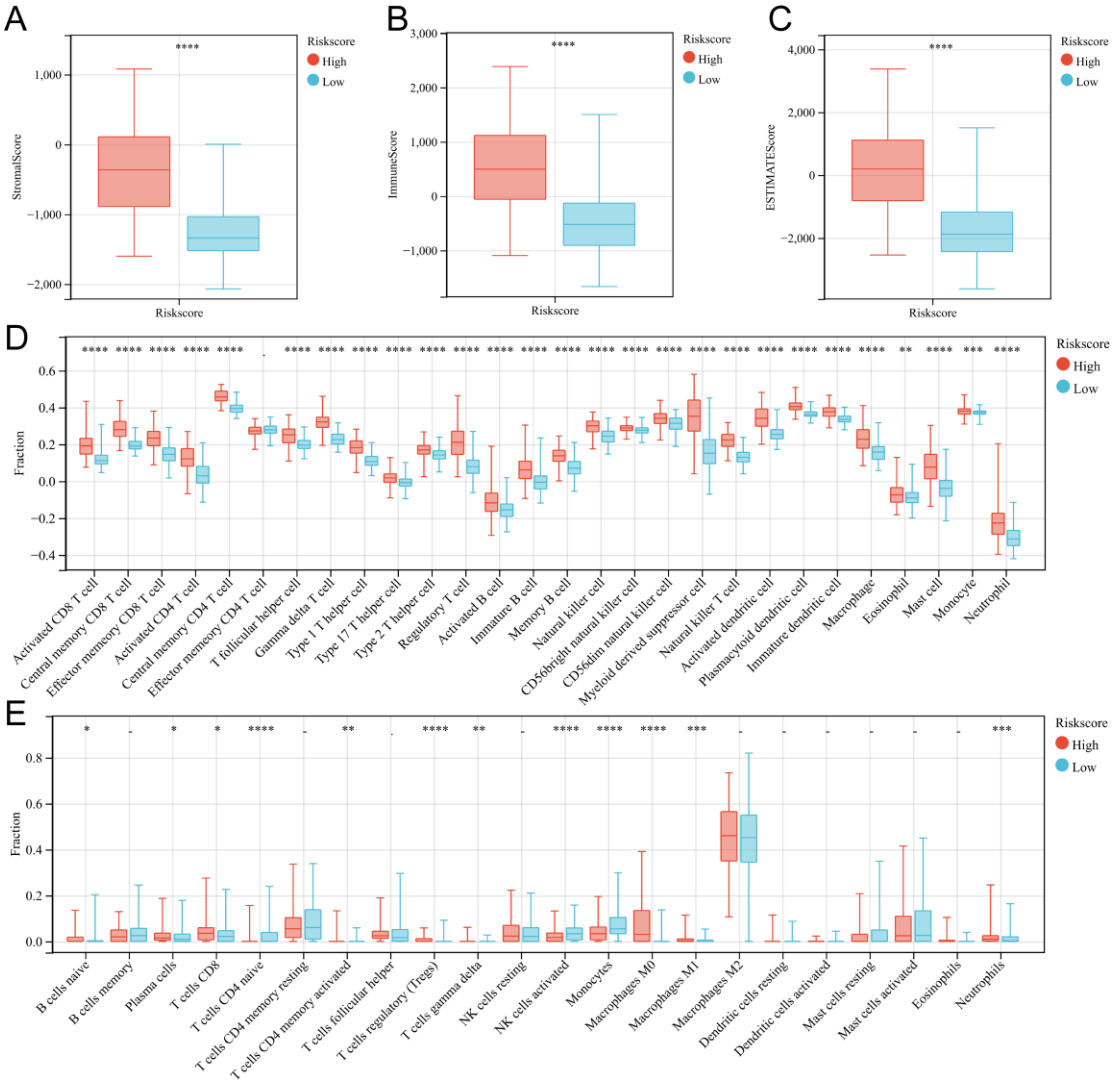

Supplementary Figure 4. Analysis of immune cell infiltration in two subgroups related to the risk score of CGGA mRNAseq325. (**A-C**) Box plot of stromal score (**A**), immune score (**B**), and ESTIMATE score (**C**) for patients in the high and low-risk score groups. (**D**)Box plot of immune cell infiltration levels high-risk score and low-risk score groups analyzed by ssGSEA. (**E**)Box plot of immune cell infiltration levels in high-risk score and low-risk score groups analyzed by CIBERSORT. *P < 0.05; **P < 0.01; ***P < 0.001, ****P < 0.0001; -, not significant.

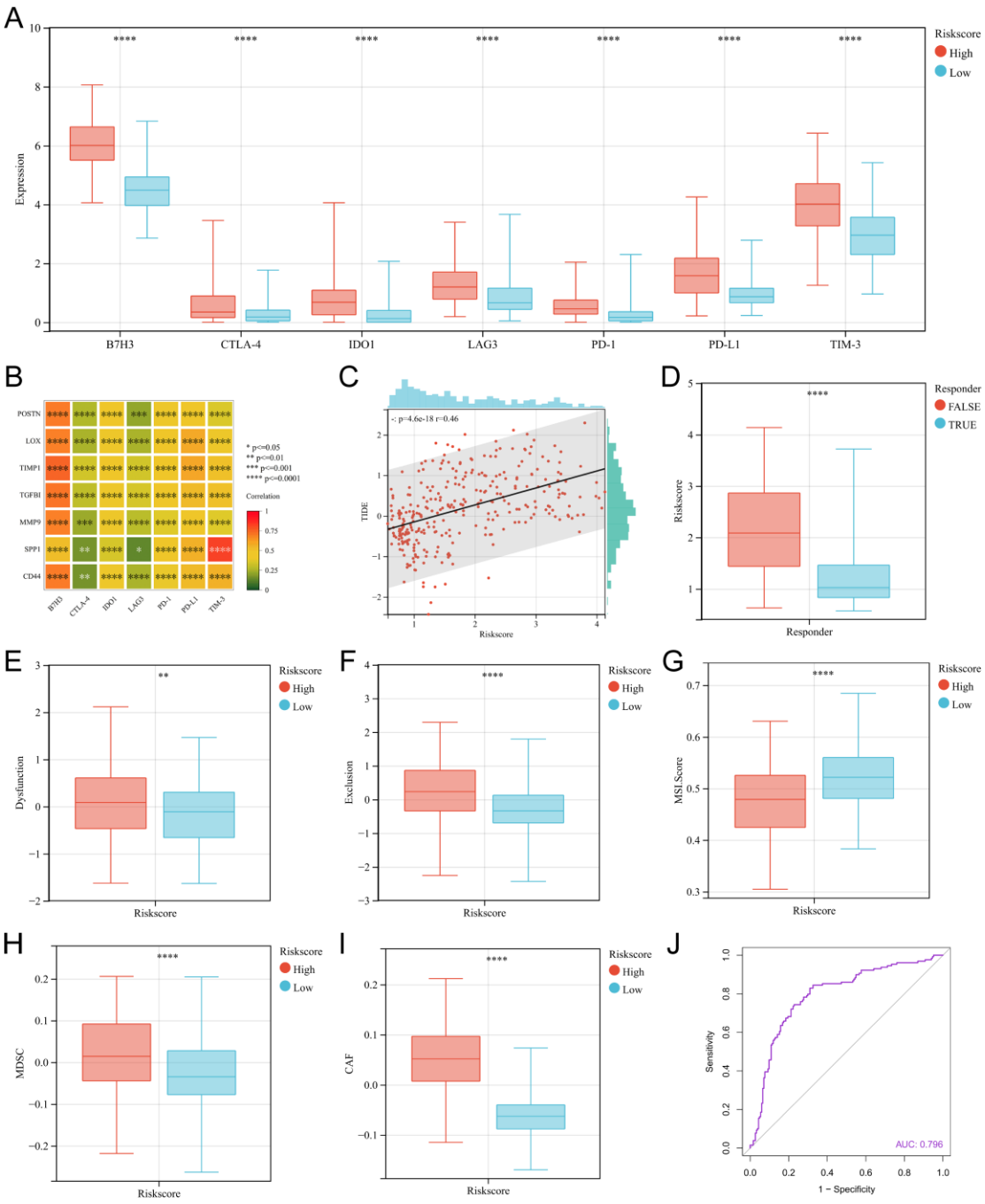

Supplementary Figure 5. The predictive role of risk model of CGGA mRNAseq325 for ICI treatment response. (**A**) Box plots of immune checkpoint expression in the high-risk score group and low-risk score group. (**B**) Correlation analysis between the expression levels of risk model-related genes and the expression levels of immune checkpoints. (**C**) Correlation analysis between the risk score and TIDE score. (**D**) Box plots of risk scores for predicting ICI treatment true responder and false responder gliomas using the TIDE algorithm. (**E**) Box plots of Dysfunction scores for high-risk score group and low-risk score group. (**F**) Box plots of Dysfunction scores for

high-risk score group and low-risk score group. (**G**) Box plot of Dysfunction scores for high-risk score group and low-risk score group. (**H**) Box plots of MDSC for high-risk score group and low-risk score group. (**I**) Box plots of CAF for high-risk score group and low-risk score group. (**J**) ROC curves of the risk score predicting response to ICI treatment.

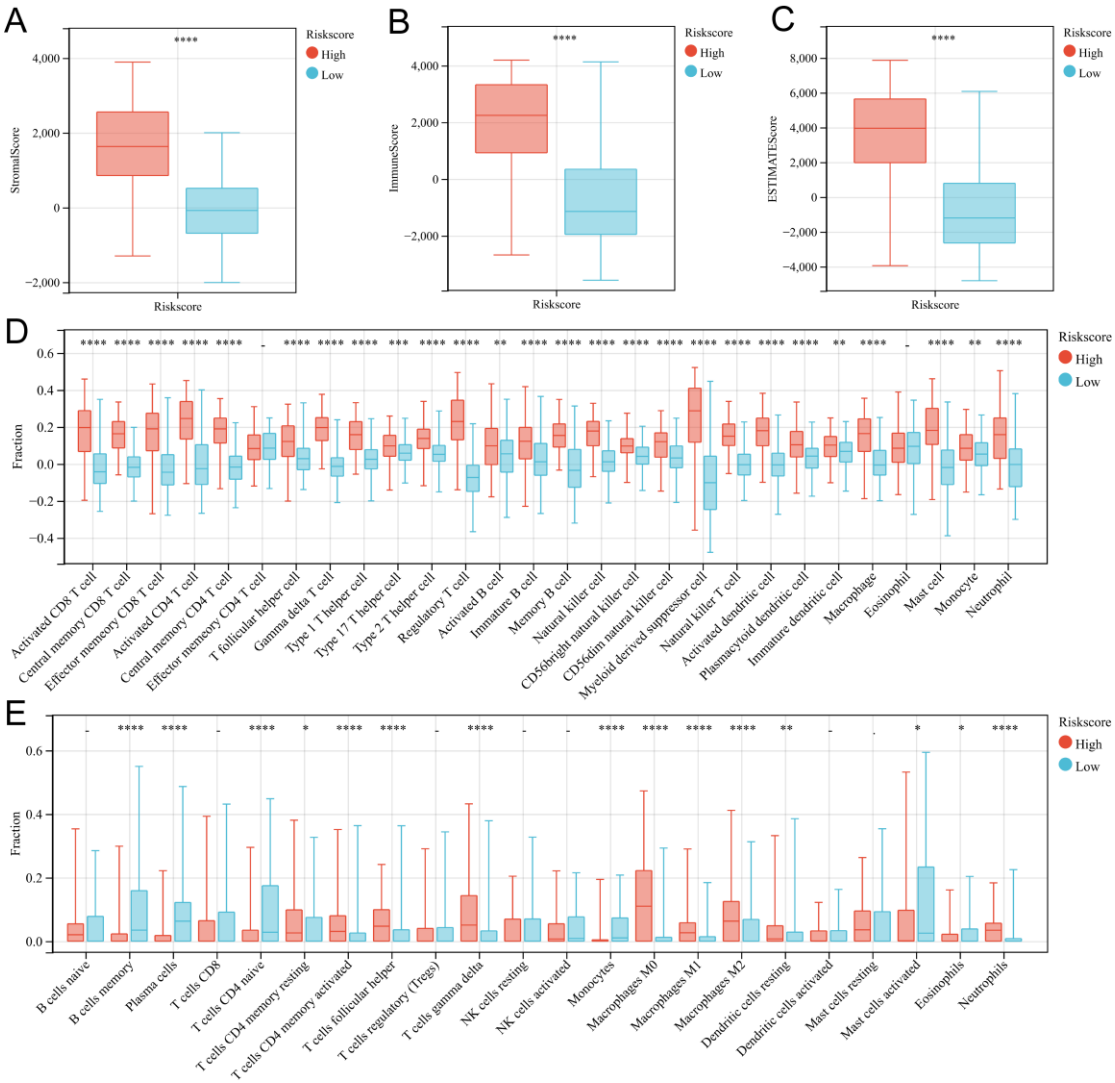

Supplementary Figure 6. Analysis of immune cell infiltration in two subgroups related to the risk score of CGGA mRNAarray. (**A-C**) Box plot of stromal score (**A**), immune score (**B**), and ESTIMATE score (**C**) for patients in the high and low-risk score groups. (**D**) Box plot of immune cell infiltration levels high-risk score and low-risk score groups analyzed by ssGSEA. (**E**) Box plot of immune cell infiltration levels in high-risk score and low-risk score groups analyzed by CIBERSORT. *P < 0.05; **P < 0.01; ***P < 0.001, ****P < 0.0001; -, not significant.

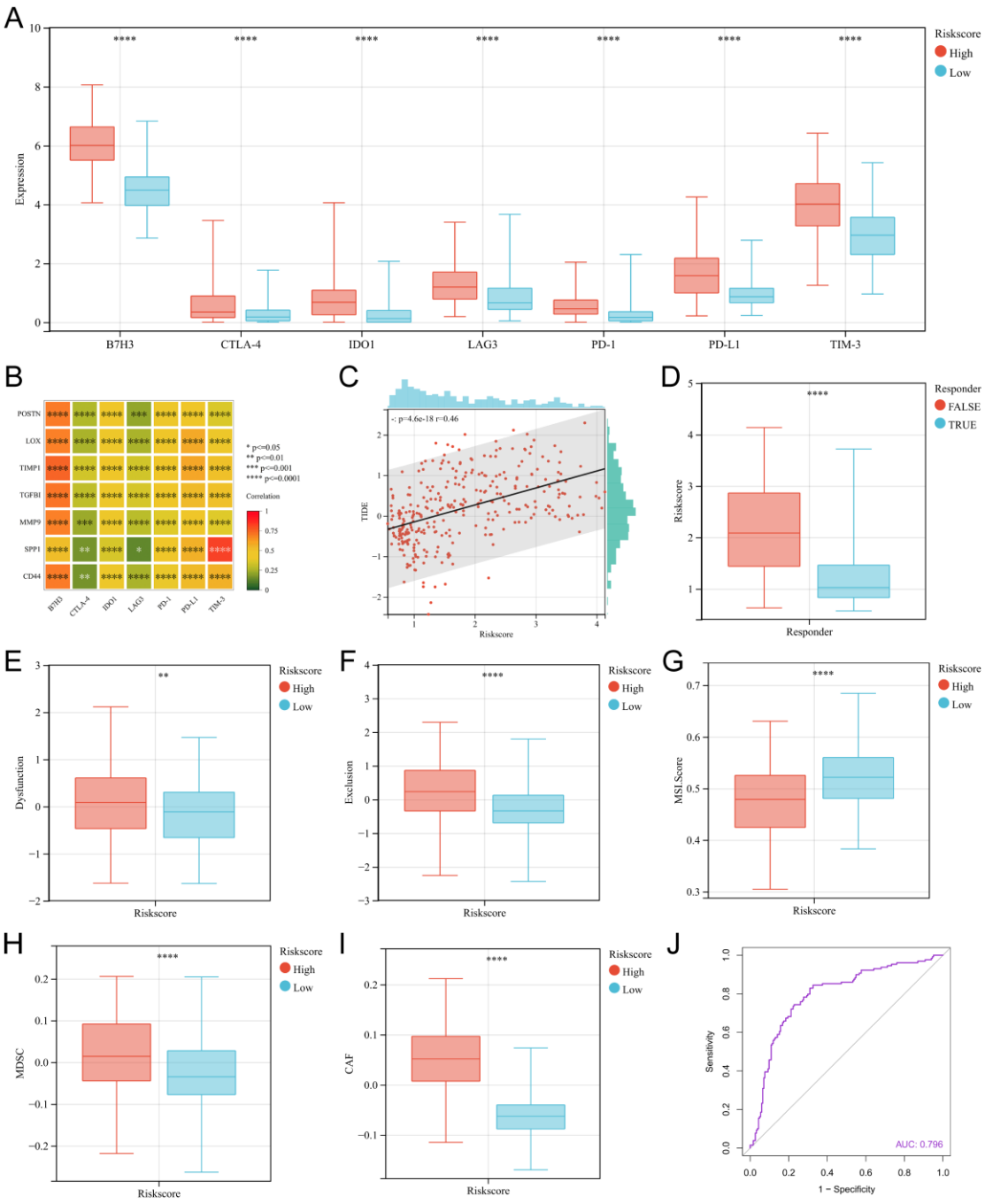

Supplementary Figure 7. The predictive role of risk model of CGGA mRNAarray for ICI treatment response. (**A**) Box plots of immune checkpoint expression in the high-risk score group and low-risk score group. (**B**) Correlation analysis between the expression levels of risk model-related genes and the expression levels of immune checkpoints. (**C**) Correlation analysis between the risk score and TIDE score. (**D**) Box plots of risk scores for predicting ICI treatment true responder and false responder gliomas using the TIDE algorithm. (**E**) Box plots of Dysfunction scores for high-risk score group and low-risk score group. (**F**) Box plots of Dysfunction scores for

high-risk score group and low-risk score group. (**G**) Box plot of Dysfunction scores for high-risk score group and low-risk score group. (**H**) Box plots of MDSC for high-risk score group and low-risk score group. (**I**) Box plots of CAF for high-risk score group and low-risk score group. (**J**) ROC curves of the risk score predicting response to ICI treatment.

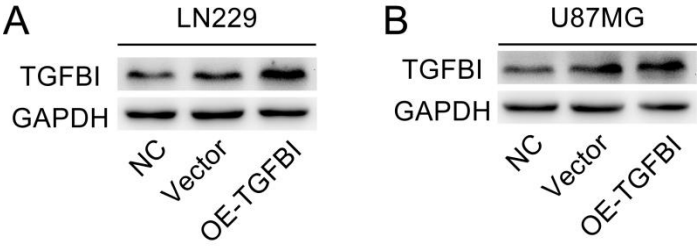

Supplementary Figure 8. The expression of TGFBI in LN229 cells and U87-MG cells after overexpression of TGFBI. (**A**) Western blot was used to detect the expression level of TGFBI in LN229 cells. (**B**) Western blot was used to detect the expression level of TGFBI in U87-MG cells.